



Lichen butyrolactone derivatives disrupt oral bacterial membrane

Alaa Sweidan, Imen Smida, Marylene Chollet-Krugler, Aurélie Sauvager, Julien Vallet, Nicolas Gouault, Nolwenn Oliviero, Zohreh Tamanai-Shacoori, Agnès Burel, Pierre van de Weghe, et al.

► To cite this version:

Alaa Sweidan, Imen Smida, Marylene Chollet-Krugler, Aurélie Sauvager, Julien Vallet, et al.. Lichen butyrolactone derivatives disrupt oral bacterial membrane. *Fitoterapia*, 2019, 137, pp.104274. 10.1016/j.fitote.2019.104274 . hal-02280840

HAL Id: hal-02280840

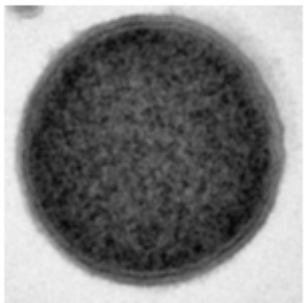
<https://univ-rennes.hal.science/hal-02280840>

Submitted on 11 Feb 2020

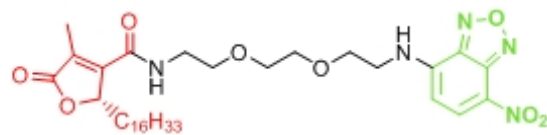
HAL is a multi-disciplinary open access archive for the deposit and dissemination of scientific research documents, whether they are published or not. The documents may come from teaching and research institutions in France or abroad, or from public or private research centers.

L'archive ouverte pluridisciplinaire **HAL**, est destinée au dépôt et à la diffusion de documents scientifiques de niveau recherche, publiés ou non, émanant des établissements d'enseignement et de recherche français ou étrangers, des laboratoires publics ou privés.

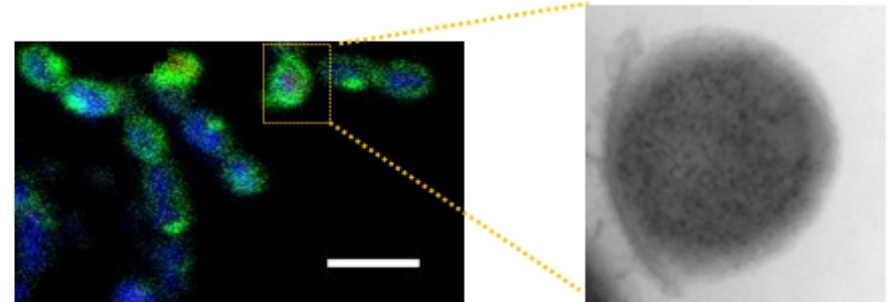
S. gordonii



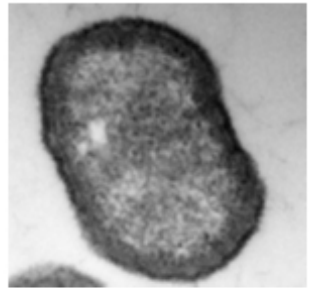
Butyrolactone derivatives



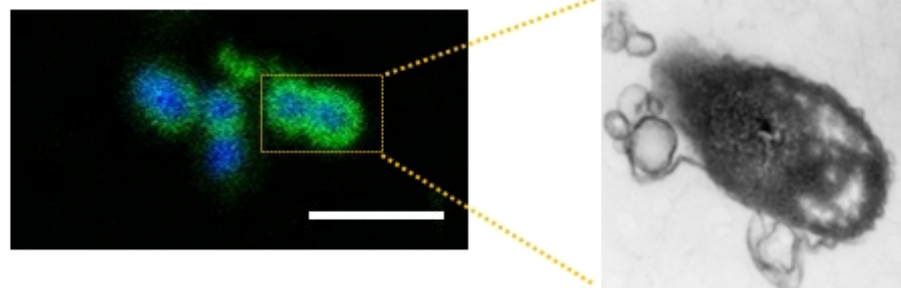
S. gordonii



Membrane disruption



P. gingivalis



P. gingivalis

1 Lichen butyrolactone derivatives disrupt oral bacterial membrane

2

3 Alaa Sweidan ^{a, c}, Imen Smida ^a, Marylène Chollet-Krugler ^b, Aurélie Sauvager ^b, Julien
4 Vallet ^b, Nicolas Gouault ^b, Nolwenn Oliviero ^a, Zohreh Tamanai-Shacoori ^a, Agnès Burel ^e,
5 Pierre van de Weghe ^d, Ali Chokr ^c, Sophie Tomasi ^b, Latifa Bousarghin ^{a,*}

6

7 ^a INSERM, Univ. Rennes, INRA, CHU Rennes, Nutrition Metabolisms and Cancer
8 (NuMeCan), UMR-1241, Biosit, MRic/ISFR, Rennes, France.

9 ^b UMR CNRS 6226, Institut des Sciences Chimiques de Rennes, Equipe CORINT, Chimie
10 Organique et Interfaces, Univ. Rennes 1, Univ. Bretagne Loire, 2 Avenue du Pr. Léon
11 Bernard, F-35043 Rennes, France

12 ^c Laboratory of Microbiology, Department of Life and Earth Sciences, Faculty of Sciences I,
13 Lebanese University, Hadath Campus, Beirut, Lebanon

14 ^d Inserm U1242, Chemistry Oncogenesis Stress Signaling (COSS), Univ. Bretagne Loire, 2
15 Avenue du Pr. Léon Bernard, F-35043 Rennes, France

16 ^e Plateforme microscopie électronique MRic, Campus Santé, Rennes 1, France

17

18 * Corresponding author. Bousarghin Latifa, U-1241 INSERM-INRA, Equipe CIMIAD, Univ.
19 Rennes 1, SFR Biosit, Université Européenne de Bretagne, Université de Rennes 1, 2 Avenue
20 du Professeur Léon Bernard, 35043 Rennes, France.

21

22 Tel.: (33) 02 23 23 48 98

23 Fax: (33) 02 23 23 49 13

24 E-mail: latifa.bousarghin@univ-rennes1.fr

25

26

27

28

29

30

31 **Abstract**

32 We have previously demonstrated that out of the butyrolactones series synthesized based on
33 the natural lichen metabolite lichesterinic acid, compound (**B-13**) was the most effective
34 against oral bacteria. However, its antibacterial mechanism is still unknown. In this study, we
35 have investigated its bacterial localization by synthesizing a fluorescently labeled **B-13** with
36 NBD while maintaining its antibacterial activity. We showed that this compound binds to
37 *Streptococcus gordonii* cell surface, as demonstrated by HPLC analysis. By adhering to cell
38 surface, **B-13** induced cell wall disruption leading to the release of bacterial constituents and
39 consequently, the death of *S. gordonii*, a Gram-positive bacterium. A Gram-negative
40 counterpart, *Porphyromonas gingivalis*, showed also cracked and ruptured cells in the
41 presence of **B-13**. Besides, we also demonstrated that the analog of **B-13**, **B-12**, has also
42 induced disruption of *P. gingivalis* and *S. gordonii*. This study revealed that butyrolactones
43 can be considered as potent antibacterial compounds against oral pathogens causing medical
44 complications.

45

46 Keywords: Lichen; Butyrolactone; *Streptococcus gordonii*; *Porphyromonas gingivalis*; cell
47 wall

48

49

50

51

52

53

54

55

56

57

58

59

60

61

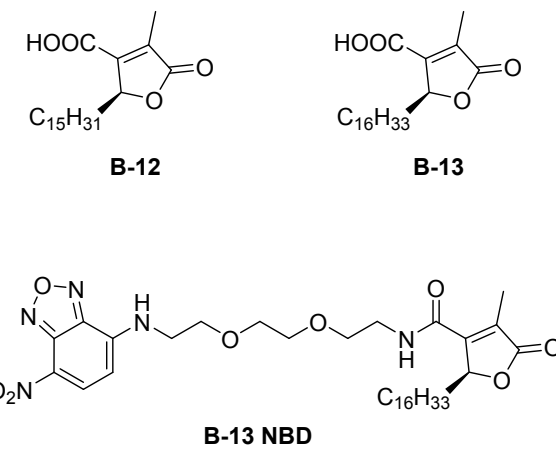
62 **1. INTRODUCTION**

63 Treatment of infections with antibiotics reduces morbidity; however, the erroneous or
64 unsuitable antibiotic can lead to the emergence of resistant pathogenic bacteria [1]. Facing
65 this worldwide concern, alternative antimicrobial candidates against multidrug-resistant
66 bacteria were developed.

67 The new drugs, which are of natural origin, are capable of surpassing the bacterial
68 resistance mechanisms [2]. Among the natural sources is the association of fungus and alga
69 and/or cyanobacterium forming a symbiotic organism named lichen which produces more
70 than 1000 distinct secondary metabolites. They were shown to be effective against sensitive
71 and several multi-drug resistant bacterial strains [3–6].

72 Among the bacteria sensitive to lichen secondary metabolites, we have previously
73 described that the synthesized butyrolactone analogs, **B-13** and **B-12** (Fig. 1), can inhibit the
74 growth of *Streptococcus gordonii* [7]. *S. gordonii* is a member of the viridans streptococci
75 large category. In the oral cavity, *S. gordonii* adheres to the salivary pellicle which coats the
76 teeth, proliferates and excretes an extracellular polysaccharide matrix protecting their
77 developing microcolony on which late colonizers will adhere. The sites provided by *S.*
78 *gordonii* are bound by *Porphyromonas gingivalis* and form a highly pathogenic complex
79 microbial community [8], [9]. *S. gordonii*, as a pioneer initial colonizer, initiates the
80 formation of dental plaques contributing in turn to the onset of dental caries and periodontal
81 diseases as well as their progression [10]. Inhibiting *S. gordonii* might block the successive
82 steps leading to acute oral diseases and introduce new antibiotics that might be able to
83 prevent and treat the periodontal diseases.

84



85

86 **Fig. 1.** Chemical structures of **B-12**, **B-13**, and **B-13 NBD**.

87 The most common way of antimicrobial killing is triggered by disruption of the
88 cytoplasmic membrane. The bacterial cell membrane is responsible for many essential
89 functions: transport, osmoregulation and respiration processes, biosynthesis and cross-linking
90 of peptidoglycan, and synthesis of lipids. It is doubtless that for all these functions,
91 membrane integrity is absolutely necessary, and its disturbance can directly or indirectly
92 cause metabolic dysfunction and cell death. Alternative mechanisms of action include
93 antimicrobial translocation into the cytoplasm where they interfere with metabolic processes,
94 such as protein synthesis or DNA replication [11]. All of these modes of action have in
95 common that the bacterial membrane will be severely damaged in the end leading to cell
96 death. One of the most validated targets for antibacterial therapy is the enzymes of
97 peptidoglycan biosynthesis. This biosynthesis is a complex process involving numerous steps
98 in the cytoplasm and the inner and outer leaflets of the cytoplasmic membrane [12], [13].

99 Antimicrobials acting at the cell wall level are the most selective compared to other
100 antibiotics. In contrast to all types of antibiotics, the cell wall-targeting ones as the
101 butyrolactones may escape from a bacterial resistant strategy in treating the oral biofilms.
102 Since the bacteria will grow significantly lower in its biofilm phase, thus, these metabolically
103 reduced-activity bacteria regarding their biosynthesis of proteins, RNA, DNA,
104 peptidoglycan, and folic acid, will be less inhibited by the antibiotics targeting these
105 processes such as ribosome and DNA topoisomerases inhibitors [14]. For example,
106 *Enterococcus faecalis* oral biofilms have been shown to require very high concentrations of
107 antibiotics such as ampicillin and vancomycin (peptidoglycan synthesis inhibitor), and
108 linezolid (protein synthesis inhibitor) [15,16]. However, targeting the cell wall can be by
109 targeting the synthesis of its components as peptidoglycan or it can be by binding directly to
110 the bacterial membrane bilayer thereby disrupting physically its integrity and its functions.
111 Hurdle et al. has mentioned also that the antimicrobials can target either the bacterial
112 membrane organization or the functions of membrane-associated respiratory enzymes [14].

113 In this study, we investigated the mechanisms of action of butyrolactone analog **B-13**
114 on two oral bacteria implicated in periodontal diseases: *S. gordonii* and *P. gingivalis*. We
115 have also compared its mechanism to another butyrolactone analog (**B-12**).
116
117
118

119 **2. Material and Methods**

120 *2.1. General chemistry*

121 All reagents of high quality were purchased from commercial suppliers and used without
122 further purification. IR spectra were obtained with PerkinElmer UATR Two infrared
123 spectrophotometer. ^1H (300 MHz) and ^{13}C (75 MHz) NMR spectra were performed on a
124 Bruker GMX 300 spectrometer. Chemical shifts were referenced to the residual solvent signal
125 (CDCl_3 ; $\delta_{\text{H}} = 7.26$, $\delta_{\text{C}} = 77.16$). The δ values are given in parts per million (ppm), and the
126 coupling constants (J values) are given in Hertz (Hz). The multiplicity of the signals is
127 reported as s (singlet), d (doublet), t (triplet), q (quadruplet), m (multiplet). ESI-HRMS were
128 carried out on a Bruker MicroTof QII spectrometer for electrospray ionization at the CRMPO
129 (Centre Régional de Mesures Physiques de l'Ouest), University of Rennes 1. Elemental
130 analyses were performed on a microanalyzer Flash EA1112 CHNS/O Thermo Electron at the
131 CRMPO. Reactions were monitored by TLC on Merk 60 F254 (0.25 mm) plates which were
132 visualized by UV detection or sprayed with KMNO_4 solutions, then heated. Log P values of
133 the compounds **B-12**, **B-13** and the probe **B-13 NBD** have been calculated using ALOGPS 2.1
134 software.

135

136 (*S*)-4-methyl-5-oxo-2-pentadecyl-2,5-dihydrofuran-3-carboxylic acid **B-12** and (*S*)-2-
137 hexadecyl-4-methyl-5-oxo-2,5-dihydrofuran-3-carboxylic acid **B-13**:

138 **B-13** and **B-12** derivatives described previously were used in this study [7]. Calculated log P
139 = 7.29 (**B-12**) and 7.67 (**B-13**)

140

141 (*2-[2-(7-Nitro-benzo[1,2,5]oxadiazol-4-ylamino)-ethoxy]-ethoxy*-ethyl)-carbamic acid
142 *tert-butyl ester 2*:

143 This compound was prepared as published [17]. Yield: 70%; red viscous oil. ^1H NMR
144 (CDCl_3 , 300 MHz) δ 1.42 (s, 9H), 3.35 (q, $J = 6,1$ Hz, 2H), 3.59 (t, $J = 6$ Hz, 2H), 3.68 (m,
145 4H), 3.85 (m, 4H), 4.98 (s, 1H), 6.19 (d, $J = 8$ Hz, 1H), 6.87 (s, 1H), 8.49 (d, $J = 8,1$ Hz, 1H)
146 ppm. ^{13}C NMR (CDCl_3 , 75 MHz) δ 28.6, 41.1, 44.4, 69.5, 70.8, 71.2, 71.3, 78.8, 100.2,
147 137.9, 145.2, 145.6, 146.1, 156.1.

148

149

150

151 *N-(2-(2-aminoethoxy)ethoxy)ethyl)-7-nitrobenzo[c][1,2,5]oxadiazol-4-amine 3:*
152 This compound was prepared as published [17] and used for the next step without any further
153 purification.

154

155

156 **Probe B-13 NBD:**

157 To a solution of **B-13** butyrolactone (44.6 mg, 0.122 mmol) and 1.28 equiv of TBTU (50.1
158 mg, 0.156 mmol) in anhydrous DMF (10 mL) under argon atmosphere, was added the NBD
159 spacer 3 (40 mg, 0.122 mmol, 1.0 equiv) and anhydrous DIEA (42.5 μ L, 0.244 mmol, 2.0
160 equiv). After stirring overnight at room temperature, the reaction was quenched by adding
161 H₂O, this solution was then extracted with diethyl ether (3 x 50 mL) and once with ethyl
162 acetate. The combined organic layers were washed with brine, dried with MgSO₄ and
163 concentrated under vacuum. The residue was purified over preparative TLC (CH₂Cl₂/EtOH
164 95:5) to yield the desired compound. Yield = 63%; dark red solid. Rf (SiO₂, CH₂Cl₂/EtOH
165 (95:5)) = 0.6. IR (ATR): ν C-O (ester) = 1133 cm⁻¹; ν C-O (lactone) = 1213 cm⁻¹; ν C=C (ar) =
166 1586 cm⁻¹; ν C=C = 1630 cm⁻¹; ν C=O (ester) = 1698 cm⁻¹; ν C=O (lactone) = 1734 cm⁻¹. ¹H
167 NMR (CDCl₃, 300 MHz) δ 0.87 (t, *J* = 6,7 Hz, 3H), 1.24 (m, 28H), 1.38 (m, 2H), 2.05 (s,
168 3H), 3.71 (m, 10H), 3.86 (t, *J* = 5,4 Hz, 2H), 5.15 (t, *J* = 5,8 Hz, 1H), 6.18 (d, *J* = 8,7 Hz,
169 1H), 6.42 (s, 1H), 6.82 (s, 1H), 8.46 (d, *J* = 8,7 Hz, 1H) ppm. ¹³C NMR (CDCl₃, 75 MHz) δ
170 10.8, 14.3, 21.2, 22.8, 25.1, 29.2, 29.3, 29.4, 29.5, 29.6, 29.7, 29.8, 29.8, 29.8, 30.2, 32.1,
171 32.9, 39.4, 43.6, 68.2, 69.7, 70.4, 70.6, 81.8, 99.1, 124.3, 129.1, 136.5, 143.8, 144.1, 153.8,
172 162.5, 171.3, 173.4 ppm. HRMS (ESI) m/z [M+Na]⁺ calcd. for C₃₄H₅₃N₅O₈Na 682,37918,
173 found 682.37920. Anal. Calcd. for C₃₄H₅₃N₅O₈ : C, 61,89; H, 8.10 ; N, 10.61. Found : C,
174 62.40 ; H, 8.06 ; N, 9.70. Calculated log P = 7.10.

175

176 *2.2. Bacterial strains*

177 We used in this study the oral bacteria, *Streptococcus gordonii* DL1 and
178 *Porphyromonas gingivalis* ATCC 33277. We have grown them in an anaerobic environment
179 (N₂-H₂-CO₂ [80:10:10]) at 37°C utilizing brain-heart infusion (BHI) medium (DIFCO,
180 France) and blood Columbia agar plates (AES Chemunex, France) supplemented with hemin
181 (5 μ g/mL) and menadione (1 μ g/mL) (Sigma Aldrich, France) [7].

182

183 2.3. Determination of the minimum inhibitory concentration and minimum bactericidal
184 concentration

185 Broth microdilution test was done as described formerly [7]. In a nutshell, 1:2 serial
186 dilutions of the butyrolactone derivatives were done in BHI medium in 96-well plate (Sterile,
187 Flat bottom, with lid, Greiner Bio-one, Germany). Doxycycline antibiotic was used as a
188 positive control [18]. The wells were inoculated with 3×10^7 CFU.ml⁻¹ of *P. gingivalis*. After
189 that, the plate is incubated anaerobically for 48 hours at 37°C. The clear well corresponding to
190 the lowest concentration was defined as the minimal inhibitory concentration or MIC. Then,
191 all the clear wells were spread on Columbia agar plates to be incubated for 5 days to uncover
192 the minimal bactericidal concentration or MBC which is the lowest concentration plate with
193 no colonial growth. The experiment was repeated three times.

194

195 2.4. Cellular localization of butyrolactone derivatives in the oral bacteria

196 2.4.1. Confocal microscopy (CLSM)

197 After inoculating 1 mL of BHI medium to have finally 3×10^7 CFU/mL of *S. gordonii* or
198 *P. gingivalis*, they were incubated anaerobically for 18 or 48 hours, respectively. Then, the
199 samples were centrifuged, the pellets were resuspended in PBS to be labeled by SYTO 40
200 and/or B-13-NBD for 15 minutes. After that, each condition was transferred into a
201 microscopic glass slide and visualized under CLSM.

202 For CLSM images, Leica-SP8 scanning microscope (Leica Microsystems, Wetzlar,
203 Germany) equipped with an inverted microscope (Fluorescence Microscopy Platform, IFR
204 140 GFAS, Université de Rennes 1) was used to visualize the slides *in situ*. The resonant
205 option with 8000 Hertz was selected to capture the images utilizing the oil immersion
206 objective lens (HC PL Apo 63X, 1.4 NA) where the numerical zoom was set at 8. The 405-
207 nm excitation laser and 430-440 nm band-pass emission filter were used for SYTO 40 and
208 the 488-nm excitation laser and 506-535 nm band-pass emission filter in case of **B-13 NBD**.

209 The confocal microscopy was also used to evaluate the bacterial viability after their
210 exposure to compound **B-13**. This viability was investigated by using two nucleic acid-
211 specific dyes: SYTO 9 which is membrane-permeable, stains all cells and can be detected by
212 green fluorescence, and propidium iodide (PI) which is membrane impermeable, stains cells
213 with damaged membranes and gives red fluorescence. Bacteria treated with **B-13** were
214 visualized *in situ* utilizing a Leica TCS-SP8 confocal laser scanning microscope (Leica

215 Microsystems, Wetzlar, Germany) equipped with an inverted microscope (Fluorescence
216 Microscopy Platform, IFR 140 GFAS, Université de Rennes I). For an entire bacterial
217 detection with the dyes, specific excitation lasers and emission filters were used. The 488-nm
218 excitation laser and 506-539 nm band-pass emission filter were utilized for SYTO 9 and the
219 561-nm excitation laser and 600-700 nm band-pass emission filter in case of PI.

220 Image acquisition and microscope piloting were done by the Leica software (LAS AF
221 V.2.2.1), and ImageJ software V1.48m (National Institute of Health) was used to analyze the
222 images.

223 *2.4.2. HPLC-DAD analysis*

224 In a 96-well plate (Sterile, Flat bottom, with lid, Biolite, Thermo Fisher Scientific, Korea)
225 containing 100 µL of BHI with or without **B-13**, 100 µL of *S. gordonii* were added into each
226 well to have a final concentration of 3×10^7 CFU/mL. A replicate for each condition was
227 prepared. After incubation under anaerobic condition at 37°C for 18 hours, the contents of
228 the MIC/2 wells were collected in an Eppendorf and extracted using an optimized protocol of
229 that described by Leejae et al. 2013 [19]. Briefly, the samples were centrifuged at 5000 rpm
230 for 10 minutes at 4 °C. The pellets obtained were washed 2 times with a buffer containing
231 (10 mM Tris.HCl of pH = 8, 0.1 mM EDTA, 1 mM DTT, 5% ethanol, and 50 mM NaCl).
232 Then, the pellets were lysed by sonication on ice for 5-10 min to be centrifuged at 5000 rpm
233 for 10 min at 4°C. Supernatants comprising the cytoplasm and the pellets containing the cell
234 wall and cell membrane were separated to be extracted by ethyl acetate. The organic upper
235 layer was transferred into a new tube to be washed with distilled water. Again, the upper
236 layer was transferred into another tube in which anhydrous sodium sulfate was added. The
237 remaining liquid was finally transferred into a new tube and evaporated to dryness for the
238 powder to be dissolved in THF. HPLC analysis were performed on a Prominence Shimadzu
239 HPLC system (Marne La Vallée, France) equipped with a C18 hypersil Gold aQ column
240 (250 x 4.6 mm, 5 µm, Thermo Scientific) and consisting of a binary pump (LC-20ADSP), a
241 surveyor autosampler (SIL-20AHT) and a diode array detector (SPD-M20A). The mobile
242 phase consisted of (H₂O + 0.1% HCOOH) as solvent A and (ACN + 0.1% HCOOH) as
243 solvent B with gradient: 0% of B during 5 min, 0%-100% of B during 5 min, 100% of B
244 during 5 min, 100%-0% of B during 5 min, 0% of B during 10 min. The flow rate was 1
245 mL/min and 20 µL of each sample were injected. DAD data were recorded at 228 and 254

246 nm and absorption spectra (210–400 nm) were recorded each second. The two samples, the
247 pellet, and supernatant of each condition, had their own HPLC chromatograms allowing us to
248 determine in which one (cell wall/cytoplasm) the butyrolactone was detected. Identification
249 of **B-13** in the samples was done by comparison of its retention time and UV-spectra with the
250 standard under the same chromatographic conditions.

251 *2.4.3. Transmission electron microscopy (TEM):*

252 Following overnight incubation, treated or untreated bacteria were collected,
253 transferred to Eppendorf tubes and washed three times in Cacodilic buffer (0.15 M, pH 7.4).
254 Fractions of bacterial suspension were fixed at 4°C for 60 min with 2% glutaraldehyde in
255 0.15 M Cacodilic buffer to be washed three times in the same buffer. Cells were post-fixed in
256 1% OsO₄ for 60 min at 4°C, rinsed in Cacodilic buffer and embedded in 2% Low melting
257 agar (Sigma). After the dehydration series in acetone, the cells samples were embedded in
258 conventional EPON (EMS 1420) and then polymerized at 60°C for 48h. Resins blocks were
259 sectioned into 80 nm ultrathin sections using ultramicrotome LEICA UC7. These sections
260 were mounted on copper grids and stained. Grids were observed using a TEM JEOL-JEM
261 1400 (Jeol Ltd, Tokyo, Japan) at an accelerating voltage of 120 kV and equipped with a
262 Gatan Inc. Orius 1000 camera.

263

264 **3. RESULTS AND DISCUSSION**

265 *3.1. Effect of butyrolactone analogs on the growth of *P. gingivalis* planktonic cells*

266 The synthesized butyrolactones were shown to be potentially active against *P.*
267 *gingivalis* where the COOH-containing compounds carrying an aliphatic chain with a minimal
268 number of 13 carbon atoms were the best (Table 1). **B-7** was the least active with MIC = 75
269 µg ml⁻¹ and no MBC. It was followed by the unsaturated compounds (**B-3** and **B-4**) or
270 saturated compounds substituted with a hydroxyl (**B-1** and **B-2**), or a vinyl group (**B-5** and **B-**
271 **6**) which exhibited moderate activity. The activity increased to reach MICs = 0.037 and 0.293
272 µg ml⁻¹ and MBCs = 1.17 and 0.586 µg ml⁻¹ for **B-12** and **B-13**, respectively. These latter
273 butyrolactones possess a conjugated carboxylic acid group and the longer aliphatic chains.
274 They were even stronger than the reference antibiotic, doxycycline which presented an MIC =
275 0.13 µg ml⁻¹ and no MBC. It is worth noting that **B-12** was more efficient than doxycycline
276 by about 3 times comparing their MICs and much more effective regarding their MBCs

277 Table 1. MIC and MBC of butyrolactones against *P. gingivalis* by broth microdilution

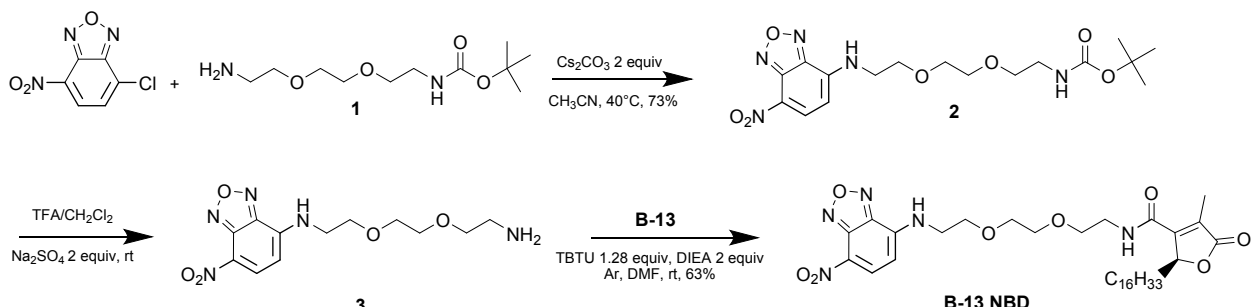
Compound	MIC ($\mu\text{g/mL}$)	MBC ($\mu\text{g/mL}$)
B-1	9.38	37.5
B-2	37.5	150
B-3	4.69	37.5
B-4	4.69	75
B-5	37.5	75
B-6	2.34	75
B-7	75	>i
B-8	9.38	150
B-9	37.5	150
B-10	0.073	9.38
B-11	0.586	4.69
B-12	0.037	1.17
B-13	0.293	0.586
Doxycycline	0.13	>i

278 >i: greater than the initial concentration

279

280 *3.2. Fluorescent B-13 butyrolactone adheres to S. gordonii membrane*281 Previously, we have demonstrated that lichen butyrolactone derivatives such as **B-13**
282 inhibit two oral bacteria *S. gordonii* [7] and *P. gingivalis* (unpublished results).283 However, further studies are needed to determine the putative mechanisms for their
284 antimicrobial activity. We were therefore interested in preparing a fluorescent tool to try to
285 elucidate their mechanism. We envisioned that this could be accomplished by using NBD, a
286 commonly used fluorescent probe as fluorophore and a pegylated diamine as a linker. So, we
287 synthesized the NBD-tagged butyrolactone **B-13** (Scheme 1). Based on a reported
288 methodology [17], the NBD-based probe **3** was obtained by anchoring *N*-Boc monoprotected
289 Pegylated diamine linker **1** to chloro-NBD in the presence of cesium carbonate in acetonitrile
290 followed by TFA mediated amine deprotection. Finally, this fluorescent probe was coupled
291 to the active substrate. For this last step, we selected a peptidic coupling reaction between the

292 probe and **B-13** (step 3). This was carried out in the presence of TBTU and DIEA in
 293 anhydrous DMF. The final **B-13 NBD** compound was thus obtained with a yield of 63%.



294
295

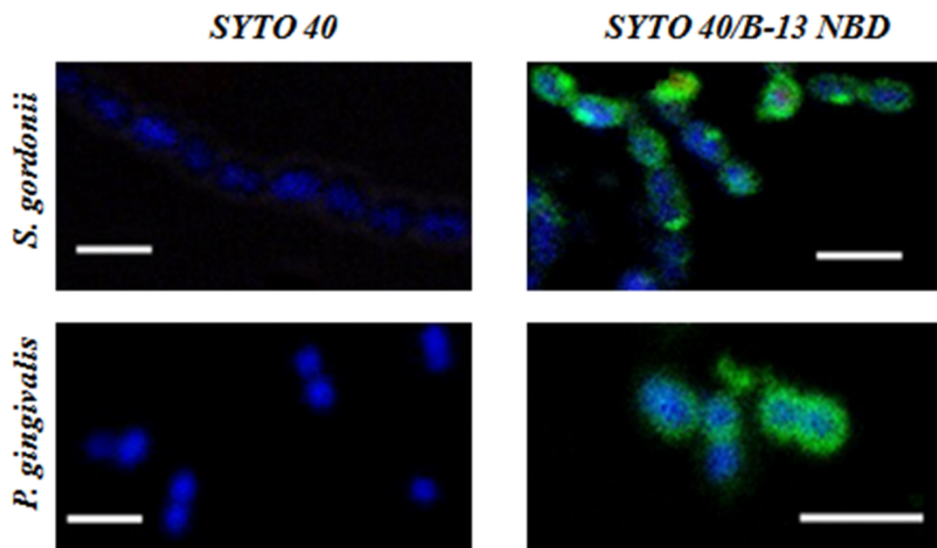
296 **Scheme 1.** Synthesis of **B-13 NBD** fluorescent probe

297 In such an approach using a fluorescent tool, one critical point is the good positioning
 298 of the probe in the active compound so that the biological activity is maintained. So, **B-13**
 299 **NBD** was evaluated ($\text{MIC} = 37.5 \mu\text{g ml}^{-1}$) and compared to **B-13** for its antimicrobial
 300 activity. Notably, the conjugation of NBD to **B-13** did not eliminate their biological activity
 301 as their antimicrobial activity against *S. gordonii* was seen. Zhao et al. 2016 [20] also have
 302 shown that NBD is a highly tolerated fluorescence label and Matijašić et al. in 2012 [21]
 303 have demonstrated that 9a-NBD-azithromycin has antimicrobial properties comparable to
 304 azithromycin. In order to compare the polarity of the probe and the active **B-12** and **B-13**
 305 compounds, their log P values have been calculated using ALOGPS 2.1 software giving a
 306 prediction of their relative lipophilicity. Regarding their Log P values (**B-13 NBD**: log P =
 307 7.10; **B-12**: log P = 7.29 and **B-13**: log P = 7.67), the three compounds appear to be highly
 308 lipophilic and display the same polarity. So the probe could be used as model to support the
 309 direct binding of **B-12** and **B-13** to the bacterial membrane.

310 After that, we have used **B-13 NBD**, NBD (7-nitrobenz-2-oxa-1,3-diazole) is a small size
 311 fluorescent probe originally introduced to label proteins through binding to their hydrophobic
 312 region, to investigate the cellular localization of **B-13** in *S. gordonii* by confocal laser
 313 scanning microscopy (CLSM). Confocal microscopic images of *S. gordonii* following the
 314 treatment of **B-13 NBD** showed green fluorescence (Fig. 2) which indicated considerable
 315 binding of this compound onto the bacteria, as seen by the presence of green fluorescence on
 316 cell membranes. The green fluorescence has surrounded the bacterial DNA stained in blue
 317 with SYTO 40, suggesting a strong localization in the cell wall. Tripathi et al. 2015 used this

318 NBD fluorescent probe to label IsCT, antimicrobial peptide, and its analogs [22]. They
319 showed that some IsCT-NBD labelled versions were accumulated onto the bacterial
320 membrane, others were translocated through *E. coli* membrane and were localized in the
321 cytoplasm. This study demonstrated that NBD did not prevent localization of molecules in
322 cytoplasm

323



324

325 **Fig. 2.** Localization of fluorescently labeled **B-13 NBD** in *S. gordonii* and *P. gingivalis* by
326 confocal microscopy. The bacterial DNA is stained by SYTO 40 in blue and **B-13 NBD**
327 adhered to the bacterial surface and appears in green. Bars represent 2 μ m.

328

329 Cellular dysfunctions can result from the interaction of an antimicrobial with the
330 microbial cell membrane [23]. The antimicrobial can only attach to the cell membrane and
331 alter its structure, permeability, and/or transport activity. On the other hand, the antimicrobial
332 can follow another pathway. After binding the cell membrane, it may penetrate inside the
333 cells and affect vital cellular functions. To determine the antibacterial mechanisms of **B-13** in
334 *S. gordonii*, localization of **B-13** in the bacteria was performed after incubating the latter with
335 the compound for 1 and 18h. Lysed bacteria were centrifuged and their cell wall and
336 membrane pellet (Fig. 3a) and cytoplasmic supernatant (Fig. 3b) fractions were analyzed
337 using HPLC. Chromatograms in Figure 3 indicated that the compound was clearly visualized

only in the cell wall and membrane fraction of the treated cells in the same manner as the control **B-13** after 1h of incubation. After 18h of treatment, a low level of **B-13** was detected in the cell membrane. This signal decrease of the compound may be caused by the degradation or the release by bacteria of this butyrolactone. In contrast, **B-13** was not detected in the cytoplasm fraction. This kinetic study suggests that **B-13** binds the membrane and does not cross to the cytoplasm.

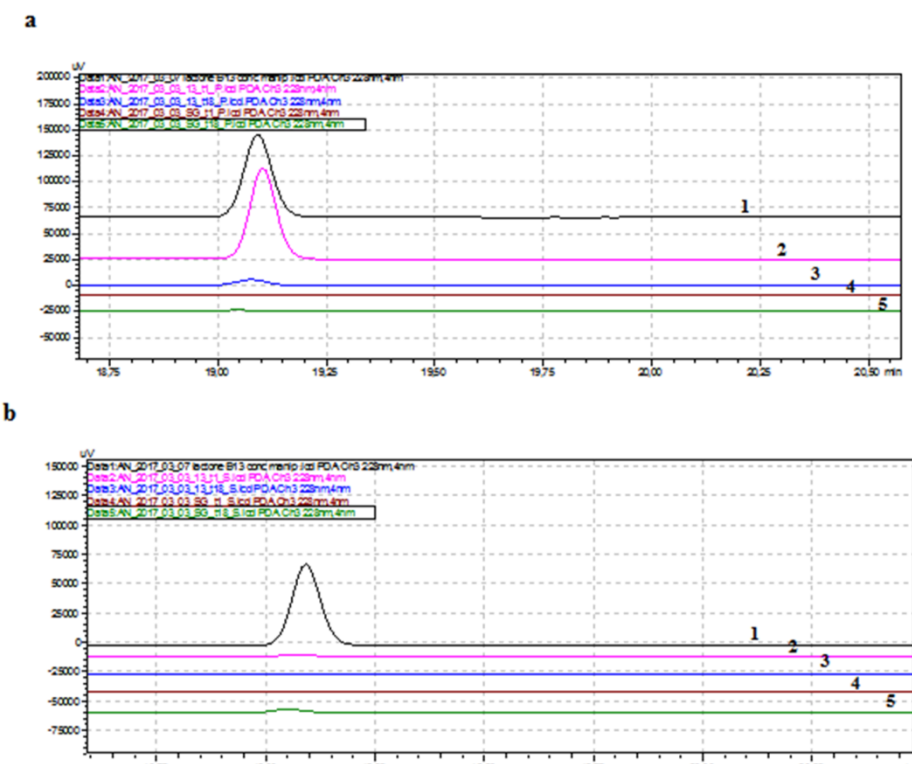


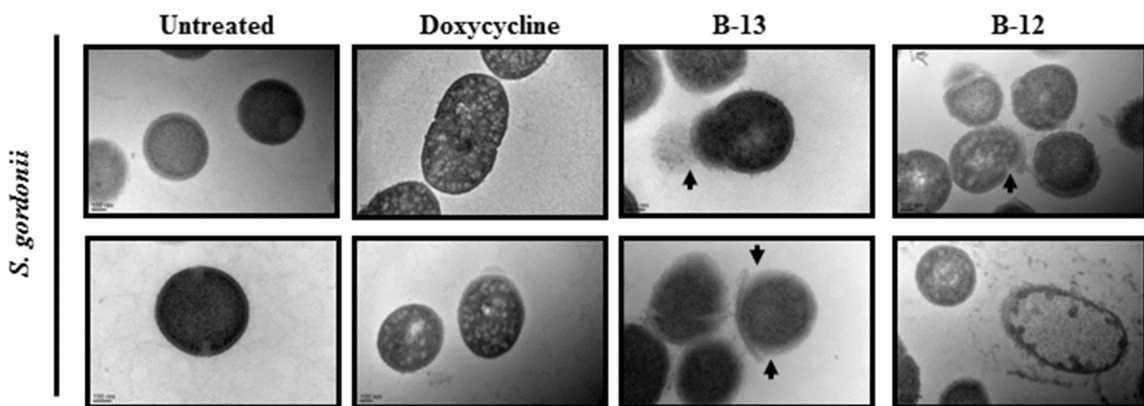
Fig. 3. Localization of **B-13** in *S. gordonii* using HPLC method. After incubation with **B-13**, *S. gordonii* was lysed, and the cell wall and cell membrane were separated from the cytoplasm by centrifugation. (a) HPLC analysis of cell wall and membrane; (b) HPLC analysis of cytoplasm. **B-13** was detected in the cell wall and membrane fraction of lysed *S. gordonii*. **B-13** as a reference (1), *S. gordonii* incubated with **B-13** for 1h (2) or 18h (3), *S. gordonii* incubated alone for 1h (4) or 18h (5).

351

352 3.3 *B-13 Butyrolactone induced cell wall disruption of S. gordonii*

353 To obtain a deeper insight into the mode of action of **B-13**, the morphology of *S. gordonii* was visualized by transmission electron microscopy (TEM) after treatment with this

355 compound (Fig. 4). Untreated bacteria appeared intact with a typically delimited cell wall
356 and well-defined membrane, and a cytoplasmic content with few electron-dense areas.
357 Treatment with doxycycline, the reference antibiotic [18], caused cytoplasmic alterations as
358 suggested by the presence of round bodies in the cytoplasm with a similar electron density
359 like clear vesicles. However, in presence of **B-13**, the bacteria appeared lysed with broken
360 walls and membranes, and heterogeneous electron density zones in the cytoplasm (Fig. 4).
361 The cells showed aberrant morphology; they were cracked and ruptured leading to their
362 death. In some cells, the externalization of cytoplasmic material could be seen by the way of
363 vesicles and rupture of the cell. Altogether, the results suggested that **B-13** inflicted
364 considerable damage to *S. gordonii* membrane and this membrane disruption property could
365 be the basis of the antibacterial activity of this compound.



366
367 **Fig. 4.** Transmission electron micrographs of *S. gordonii*. **B-13**, as **B-12**, disrupted *S. gordonii*
368 cell wall (as indicated by black arrows).

369 Furthermore, we have counted the damaged bacterial cells upon treatment with
370 butyrolactones or doxycycline in three random regions from the electron micrographs of each
371 condition and calculated their percentages (Table 2). *P. gingivalis* was shown to be more
372 sensitive than *S. gordonii*, and this coincides with our results from the microdilution test.
373 Butyrolactones had similar values which were higher than doxycycline by 1.5 to 2 times.

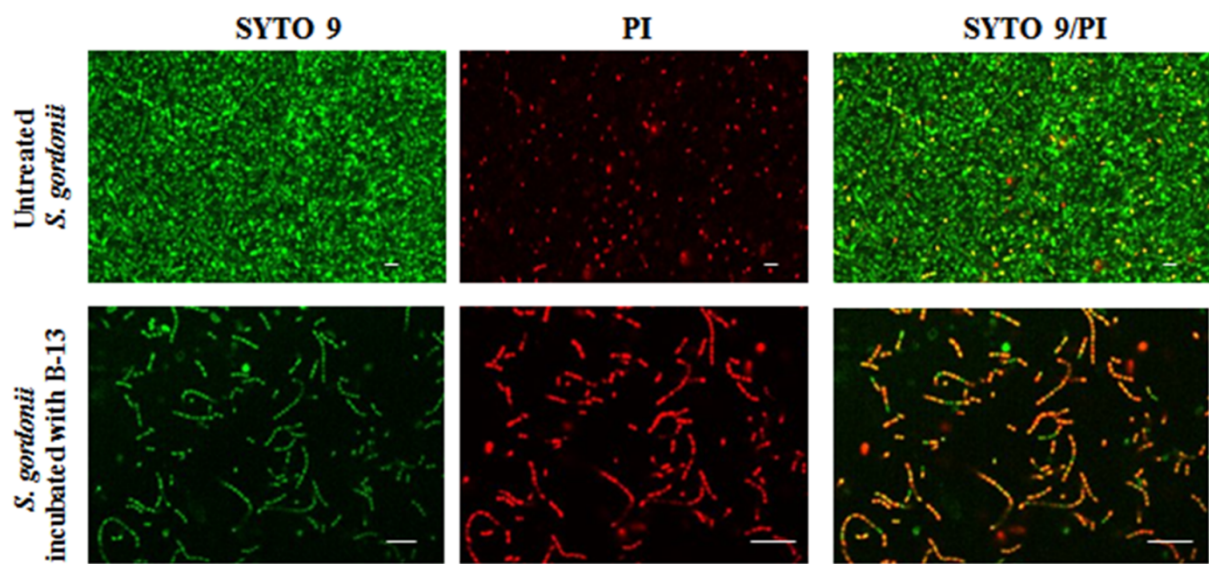
374

375

376 Table 2. Percentage of damaged bacterial cells upon treatment with butyrolactones or
 377 doxycycline (enumerated in the transmission electron micrographs).

	<i>S. gordonii</i>	<i>P. gingivalis</i>
B-12	58.5±1.3	92.5±2.8
B-13	55.7±1.6	86.1±3.1
Doxycycline	32.6±2.6	66.4±1.2

378 CLSM analysis was used to provide further confirmation of our hypothesis on this
 379 membrane disruption. In order to follow permeability modification due to **B-13** exposure, we
 380 monitored the fluorescence intensity of bacterial culture mixed with propidium iodide (PI)
 381 and SYTO 9 [24]. SYTO 9 can penetrate intact or damaged membranes giving green
 382 fluorescence, however, PI fluoresces in red and can only penetrate damaged membranes. As
 383 a result, the dead cells have appeared nearly in orange color due to the presence of the two
 384 labels. As shown in figure 5, untreated control *S. gordonii* cells appeared predominantly
 385 green (demonstrating living cells); whereas the **B-13** treated cells appeared substantially red,
 386 indicating the high permeability of PI dye and that most of the cells were dead. This result
 387 confirmed that **B-13** had a destructive effect on the cell membranes where the majority of the
 388 bacteria were dead.

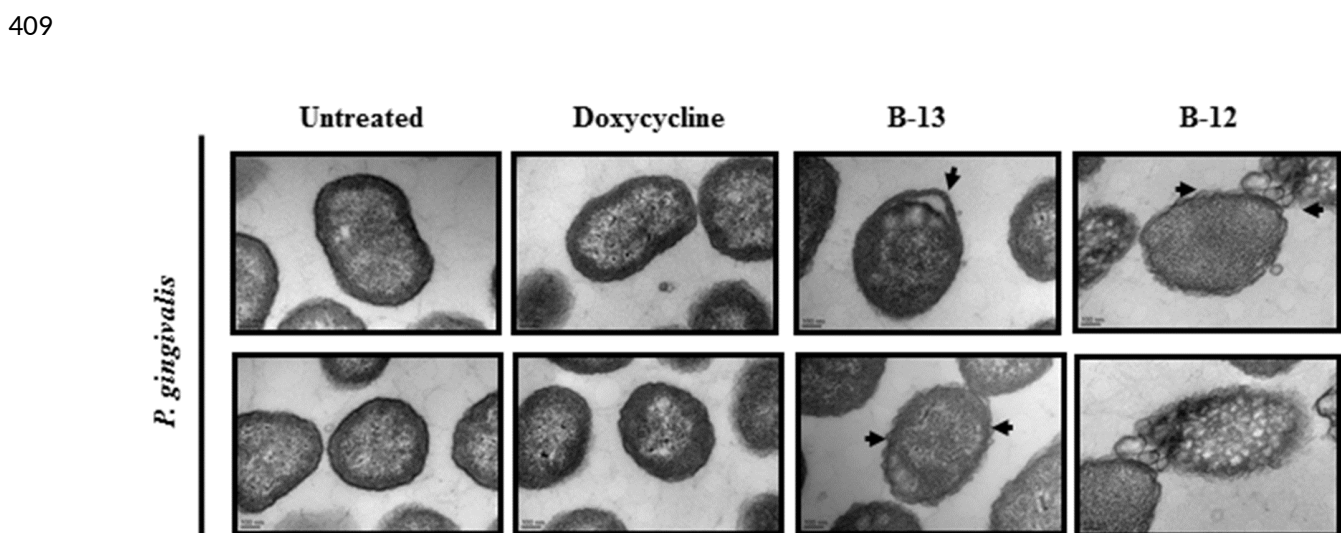


389

390 **Fig. 5.** *S. gordonii* cell suspension, untreated or treated with **B-13**, stained with SYTO 9 and
391 PI, and analyzed by CLSM. Cells with intact membranes were stained with green
392 fluorescence, whereas cells with ruptured membranes were stained with red fluorescence. The
393 overlap of the two stains appears in orange. Bars represent 10 μ m.

394
395 3.4 *B-13 Butyrolactone has also disrupted the Gram-negative bacterial membrane of P.*
396 *gingivalis*

397 In order to determine if its antimicrobial potential is influenced by the cell wall
398 composition of the microorganisms, we have investigated the effect of **B-13** on *P. gingivalis*,
399 a Gram-negative strain. When we used **B-13 NBD** on *P. gingivalis* (Fig. 2), we have
400 observed a prominent green fluorescence on cell membranes. Figure 6 showed TEM
401 micrograph of *P. gingivalis* control with a typical cell wall, outer and cytoplasmic
402 membrane, periplasmic space and cytoplasmic content with few electron-dense areas. When
403 *P. gingivalis* was treated with **B-13**, cells were damaged showing either localized or
404 complete separation of the cell membrane from the cell wall. The cellular degradation was
405 also accompanied by electron-translucent cytoplasm and cellular disruption in the damaged
406 cells. These differences in structure, thickness, and composition of the cell can explain why
407 Gram-positive *S. gordonii* were less inhibited and Gram-negative *P. gingivalis* showed
408 substantial inhibition even at lower antibiotic concentration.



411 **Fig. 6.** Transmission electron micrographs of *P. gingivalis*. **B-13**, as **B-12**, disrupted *P.*
412 *gingivalis* cell wall (as indicated by black arrows).

413

414 3.5 *B*-13 Butyrolactone analog, **B**-12, has also disrupted the membrane of oral bacteria

415 In order to determine if this membrane disruption is specific to the synthesized
416 butyrolactone, we have used an analog of **B**-13, **B**-12 with a shorter aliphatic chain (Fig. 1),
417 which we have already described in Sweidan et al. 2016 [7]. Electron Micrographs of *S.*
418 *gordonii* or *P. gingivalis* treated with **B**-12 showed broken membrane and dead bacteria (Fig.
419 4 and Fig. 6). However, as for **B**-13, we found that the effect of **B**-12 is also more active
420 against Gram-negative as seen by the formation of unwinded structures in the cell wall,
421 irregularly shaped cells, and scratched cell surface of *P. gingivalis* (Fig. 6).

422 The finding that **B**-12 has the ability to break and damage the bacterial membrane
423 leads to propose that the bactericidal effect of our synthesized butyrolactones is based on
424 destroying the cell surface of bacteria.

425

426 4. Conclusion

427 *S. gordonii* and *P. gingivalis* are oral bacteria initiating the formation of dental plaques
428 contributing in turn to the onset of dental caries and periodontal diseases as well as their
429 progression [10]. We have previously demonstrated that these bacteria are sensitive to new
430 drugs which are of natural origin as they are derived from lichen secondary metabolites
431 [7,25]. However, its antibacterial mechanisms are still unknown. By using the compound (**B**-
432 **13**) which is one of the most active butyrolactones series synthesized based on the natural
433 compound, lichesterinic acid, we have shown that this compound has bound to the bacterial
434 surface and induced membrane modification breaking the cell wall and releasing the
435 cytoplasmic constituents leading to bacterial death. These results suggested that its
436 antimicrobial potential is influenced by the composition of the cell wall of the
437 microorganisms [26].

438 This study shows for the first time the mechanism of action of synthesized
439 butyrolactones, analogs of lichesterinic acid. To our knowledge, there are only two studies on
440 the mechanism of action of lichen-derived compounds [27], [3]. Gupta et al. (2012)
441 demonstrated that usnic acid, a commonly occurring polyphenolic compound in many
442 species of lichens, can destabilize the membrane integrity of Methicillin-Resistant
443 *Staphylococcus aureus* (MRSA) [27]. Shrestha et al. 2016 demonstrated also that *L. vulpina*

444 extracts disrupted the integrity of MRSA membranes and targeted its cell division processes
445 in MRSA [28]. These studies have only investigated Gram-positive strains whereas both
446 Gram types were investigated in the present study.

447 Our study opens the door for future mechanistic research on lichen secondary
448 metabolites which will give a better understanding of lichen as an association of fungus and
449 alga and/or cyanobacterium forming a symbiotic organism and how to use its secondary
450 metabolites as antibiotics. In addition, the structures of the butyrolactone analogs are
451 different from those of all the antibiotics discovered to date including the cell wall-targeting
452 ones. This fact supported by the way these compounds target the bacteria as described in our
453 study, may introduce a new generation of antibiotics with a new mode of action. However, to
454 better develop a new antibiotic, it is necessary to make further investigations on lichen
455 secondary metabolites in general and **B-13** in particular.

456 **Conflicts of interest**

457 The authors declare no conflicts of interest.

458

459 **Acknowledgments**

460 We would like to acknowledge C. Le Lann, (NUMECAN – Rennes I University, France),
461 Marie Thérèse Lavault (Plateforme microscopie électronique MRic, Campus Santé, Rennes
462 1, France) and Stephanie Dutertre (Plateforme Microscopie, Biosit, Campus Santé, Rennes 1,
463 France) for their technical help in CLSM.

464 **Funding**

465

466 Rennes I University, UMR CNRS 6226 (France), and Association of Specialization and
467 Scientific Orientation (Lebanon) were behind supporting this research.

468

469

470

471

472

473 **REFERENCES**

- 474 [1] O. Özgenç, Methodology in improving antibiotic implementation policies, *World J.*
475 *Methodol.* 6 (2016) 143–153. doi:10.5662/wjm.v6.i2.143.
- 476 [2] A. Borges, A. Abreu, C. Dias, M. Saavedra, F. Borges, M. Simões, New perspectives on
477 the use of phytochemicals as an emergent strategy to control bacterial infections
478 including biofilms, *Molecules.* 21 (2016) 877. doi:10.3390/molecules21070877.
- 479 [3] G. Shrestha, L.L. St. Clair, Lichens: a promising source of antibiotic and anticancer
480 drugs, *Phytochem. Rev.* 12 (2013) 229–244. doi:10.1007/s11101-013-9283-7.
- 481 [4] J. Boustie, M. Grube, Lichens-a promising source of bioactive secondary metabolites,
482 *Plant Genet. Resour. Charact. Util.* 3 (2005) 273–287. doi:10.1079/PGR200572.
- 483 [5] V. Shukla, G.P. Joshi, M.S.M. Rawat, Lichens as a potential natural source of bioactive
484 compounds: a review, *Phytochem. Rev.* 9 (2010) 303–314. doi:10.1007/s11101-010-
485 9189-6.
- 486 [6] M. Bačkorová, R. Jendželovský, M. Kello, M. Bačkor, J. Mikeš, P. Fedoročko, Lichen
487 secondary metabolites are responsible for induction of apoptosis in HT-29 and A2780
488 human cancer cell lines, *Toxicol. Vitro Int. J. Publ. Assoc. BIBRA.* 26 (2012) 462–468.
489 doi:10.1016/j.tiv.2012.01.017.
- 490 [7] A. Sweidan, M. Chollet-Krugler, P. van de Weghe, A. Chokr, S. Tomasi, M. Bonnaure-
491 Mallet, L. Bousarghin, Design, synthesis and biological evaluation of potential
492 antibacterial butyrolactones, *Bioorg. Med. Chem.* 24 (2016) 5823–5833.
493 doi:10.1016/j.bmc.2016.09.040.
- 494 [8] K.Y. How, K.P. Song, K.G. Chan, *Porphyromonas gingivalis:* An Overview of
495 Periodontopathic Pathogen below the Gum Line, *Front. Microbiol.* 7 (2016) 53.
496 doi:10.3389/fmicb.2016.00053.
- 497 [9] P.P.C. Pita, J.A. Rodrigues, C. Ota-Tsuzuki, T.F. Miato, E.G. Zenobio, G. Giro, L.C.
498 Figueiredo, C. Gonçalves, S.A. Gehrke, A. Cassoni, J.A. Shibli, Oral Streptococci
499 Biofilm Formation on Different Implant Surface Topographies, *BioMed Res. Int.* 2015
500 (2015) 159625. doi:10.1155/2015/159625.
- 501 [10] H.M. Ng, L.X. Kin, S.G. Dashper, N. Slakeski, C.A. Butler, E.C. Reynolds, Bacterial
502 interactions in pathogenic subgingival plaque, *Microb. Pathog.* 94 (2016) 60–69.
503 doi:10.1016/j.micpath.2015.10.022.
- 504 [11] F. Guilhelmelli, N. Vilela, P. Albuquerque, L. da S. Derengowski, I. Silva-Pereira, C.M.
505 Kyaw, Antibiotic development challenges: the various mechanisms of action of
506 antimicrobial peptides and of bacterial resistance, *Front. Microbiol.* 4 (2013) 353.
507 doi:10.3389/fmicb.2013.00353.
- 508 [12] J. van Heijenoort, Recent advances in the formation of the bacterial peptidoglycan
509 monomer unit, *Nat. Prod. Rep.* 18 (2001) 503–519.
- 510 [13] A. Typas, M. Banzhaf, C.A. Gross, W. Vollmer, From the regulation of peptidoglycan
511 synthesis to bacterial growth and morphology, *Nat. Rev. Microbiol.* 10 (2011) 123–136.
512 doi:10.1038/nrmicro2677.
- 513 [14] J.G. Hurdle, A.J. O'Neill, I. Chopra, R.E. Lee, Targeting bacterial membrane function:
514 an underexploited mechanism for treating persistent infections, *Nat. Rev. Microbiol.* 9
515 (2011) 62–75. doi:10.1038/nrmicro2474.
- 516 [15] B. Kouidhi, Y.M.A. Al Qurashi, K. Chaieb, Drug resistance of bacterial dental biofilm
517 and the potential use of natural compounds as alternative for prevention and treatment,
518 *Microb. Pathog.* 80 (2015) 39–49. doi:10.1016/j.micpath.2015.02.007.
- 519 [16] K. Lewis, Platforms for antibiotic discovery, *Nat. Rev. Drug Discov.* 12 (2013) 371–
520 387. doi:10.1038/nrd3975.

- 521 [17] S. Noël, L. Guillon, I.J. Schalk, G.L.A. Mislin, Synthesis of Fluorescent Probes Based
522 on the Pyochelin Siderophore Scaffold, Org. Lett. 13 (2011) 844–847.
523 doi:10.1021/o11028173.
- 524 [18] J.H. Park, J.-K. Lee, H.-S. Um, B.-S. Chang, S.-Y. Lee, A periodontitis-associated
525 multispecies model of an oral biofilm, J. Periodontal Implant Sci. 44 (2014) 79.
526 doi:10.5051/jpis.2014.44.2.79.
- 527 [19] S. Leejae, P.W. Taylor, S.P. Voravuthikunchai, Antibacterial mechanisms of
528 rhodomyrtone against important hospital-acquired antibiotic-resistant pathogenic
529 bacteria, J. Med. Microbiol. 62 (2013) 78–85. doi:10.1099/jmm.0.049205-0.
- 530 [20] C. Zhao, A. Fernandez, N. Avlonitis, G. Vande Velde, M. Bradley, N.D. Read, M.
531 Vendrell, Searching for the Optimal Fluorophore to Label Antimicrobial Peptides, ACS
532 Comb. Sci. 18 (2016) 689–696. doi:10.1021/acscombsci.6b00081.
- 533 [21] M. Matijašić, V. Munić Kos, K. Nujić, S. Čužić, J. Padovan, G. Kragol, S. Alihodžić, B.
534 Mildner, D. Verbanac, V. Eraković Haber, Fluorescently labeled macrolides as a tool for
535 monitoring cellular and tissue distribution of azithromycin, Pharmacol. Res. 66 (2012)
536 332–342. doi:10.1016/j.phrs.2012.06.001.
- 537 [22] J.K. Tripathi, M. Kathuria, A. Kumar, K. Mitra, J.K. Ghosh, An unprecedented
538 alteration in mode of action of IsCT resulting its translocation into bacterial cytoplasm
539 and inhibition of macromolecular syntheses, Sci. Rep. 5 (2015) 9127.
540 doi:10.1038/srep09127.
- 541 [23] J.A. Tennesen, Molecular evolution of animal antimicrobial peptides: widespread
542 moderate positive selection, J. Evol. Biol. 18 (2005) 1387–1394. doi:10.1111/j.1420-
543 9101.2005.00925.x.
- 544 [24] D.J. Arndt-Jovin, T.M. Jovin, Fluorescence labeling and microscopy of DNA, Methods
545 Cell Biol. 30 (1989) 417–448.
- 546 [25] B. Gökalsin, N.C. Sesal, Lichen secondary metabolite evernic acid as potential quorum
547 sensing inhibitor against *< i>Pseudomonas aeruginosa< /i>*, World J. Microbiol.
548 Biotechnol. 32 (2016). doi:10.1007/s11274-016-2105-5.
- 549 [26] N. Malanovic, K. Lohner, Gram-positive bacterial cell envelopes: The impact on the
550 activity of antimicrobial peptides, Biochim. Biophys. Acta. 1858 (2016) 936–946.
551 doi:10.1016/j.bbamem.2015.11.004.
- 552 [27] V.K. Gupta, S. Verma, S. Gupta, A. Singh, A. Pal, S.K. Srivastava, P.K. Srivastava, S.C.
553 Singh, M.P. Darokar, Membrane-damaging potential of natural L-(–)-usnic acid in
554 *Staphylococcus aureus*, Eur. J. Clin. Microbiol. Infect. Dis. Off. Publ. Eur. Soc. Clin.
555 Microbiol. 31 (2012) 3375–3383. doi:10.1007/s10096-012-1706-7.
- 556 [28] G. Shrestha, A. Thompson, R. Robison, L.L. St Clair, Letharia vulpina, a vulpinic acid
557 containing lichen, targets cell membrane and cell division processes in methicillin-
558 resistant *Staphylococcus aureus*, Pharm. Biol. 54 (2016) 413–418.
559 doi:10.3109/13880209.2015.1038754.
- 560

Figures captions

Scheme 1. Synthesis of **B-13 NBD** fluorescent probe.

Fig. 1. Chemical structures of **B-12**, **B-13**, and **B-13 NBD**.

Fig. 2. Localization of fluorescently labeled **B-13 NBD** in *S. gordonii* and *P. gingivalis* by confocal microscopy. The bacterial DNA is stained by SYTO 40 in blue and **B-13 NBD** adhered to the bacterial surface and appears in green. Bars represent 2 μ m.

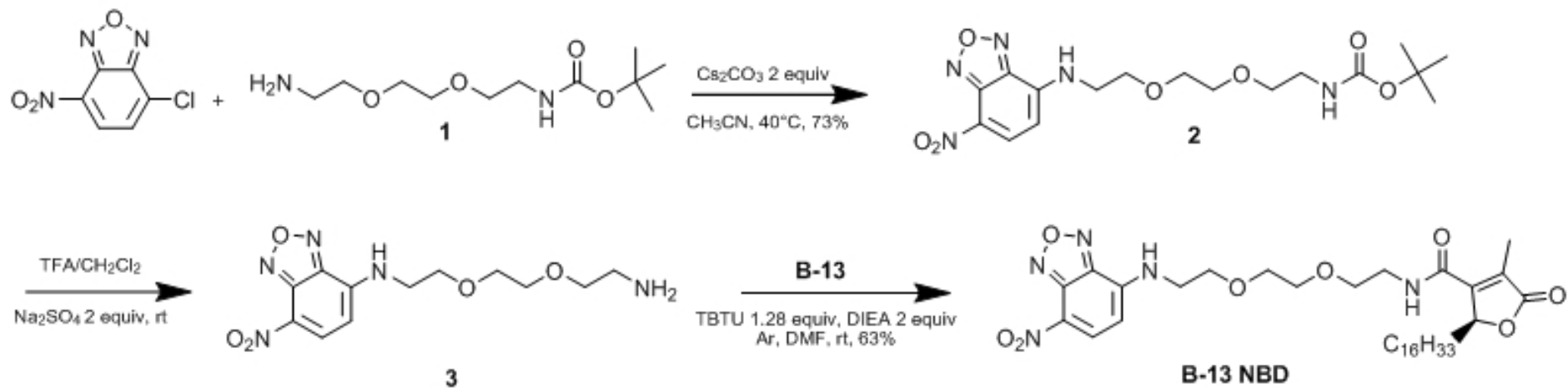
Fig. 3. Localization of **B-13** in *S. gordonii* using HPLC method. After incubation with **B-13**, *S. gordonii* was lysed, and the cell wall and cell membrane were separated from the cytoplasm by centrifugation. (a) HPLC analysis of cell wall and membrane; (b) HPLC analysis of cytoplasm. **B-13** was detected in the cell wall and membrane fraction of lysed *S. gordonii*. **B-13** as a reference (1), *S. gordonii* incubated with **B-13** for 1h (2) or 18h (3), *S. gordonii* incubated alone for 1h (4) or 18h (5).

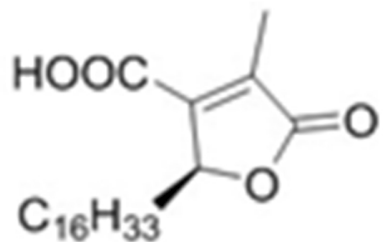
Fig. 4. Transmission electron micrographs of *S. gordonii*. **B-13**, as **B-12**, disrupted *S. gordonii* cell wall (as indicated by black arrows).

Fig. 5. *S. gordonii* cell suspension, untreated or treated with **B-13**, stained with SYTO 9 and PI, and analyzed by CLSM. Cells with intact membranes were stained with green fluorescence, whereas cells with ruptured membranes were stained with red fluorescence. The overlap of the two stains appears in orange. Bars represent 10 μ m.

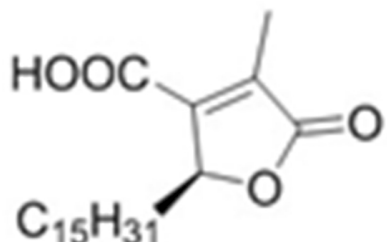
Fig. 6. Transmission electron micrographs of *P. gingivalis*. **B-13**, as **B-12**, disrupted *P. gingivalis* cell wall (as indicated by black arrows).

Scheme 1

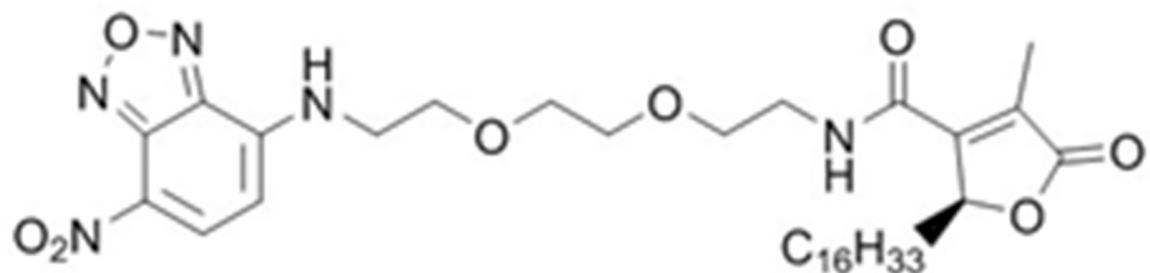




B-13



B-12

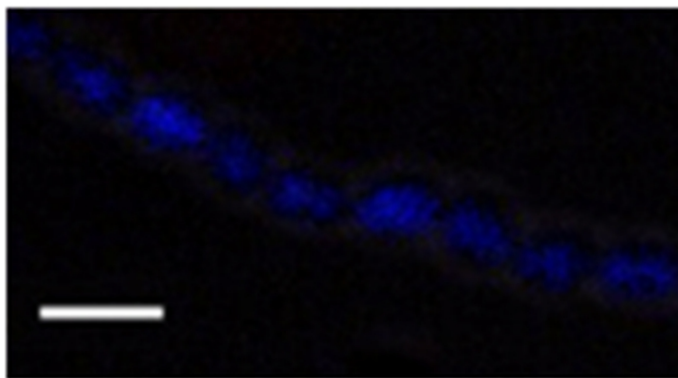


B-13 NBD

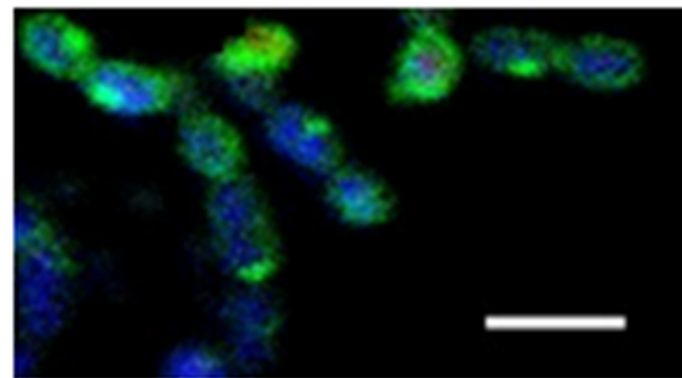
Fig. 1.

S. gordonii

SYTO 40



SYTO 40/B-13 NBD



P. gingivalis

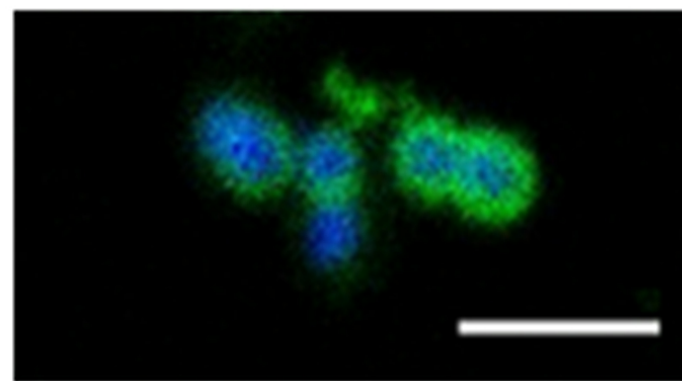
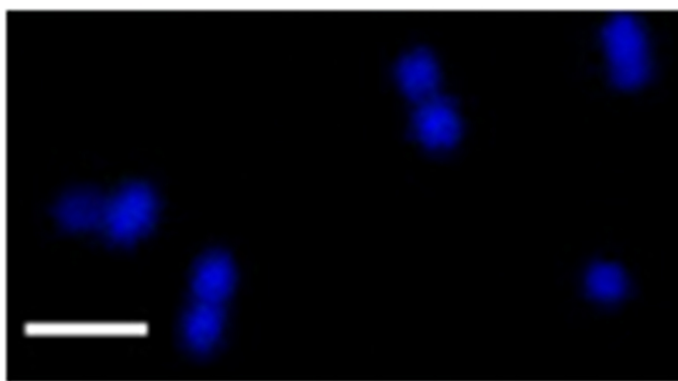
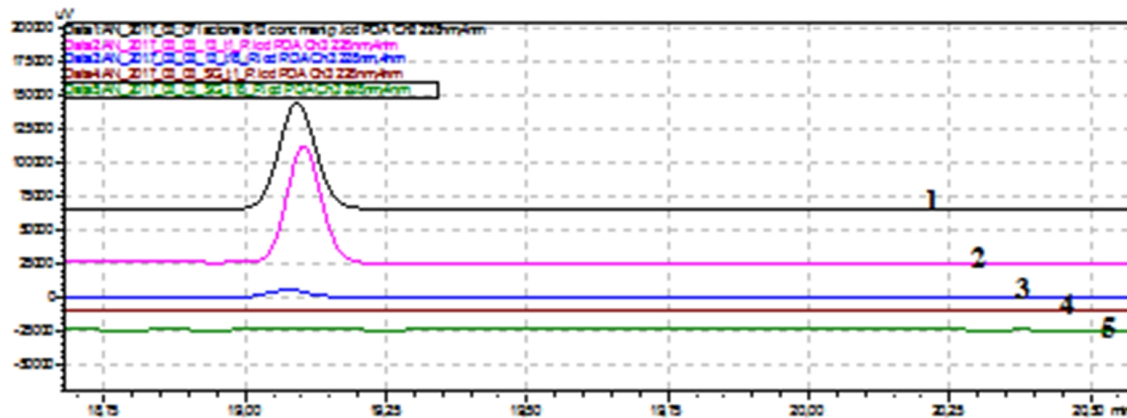


Fig. 2.

a



b

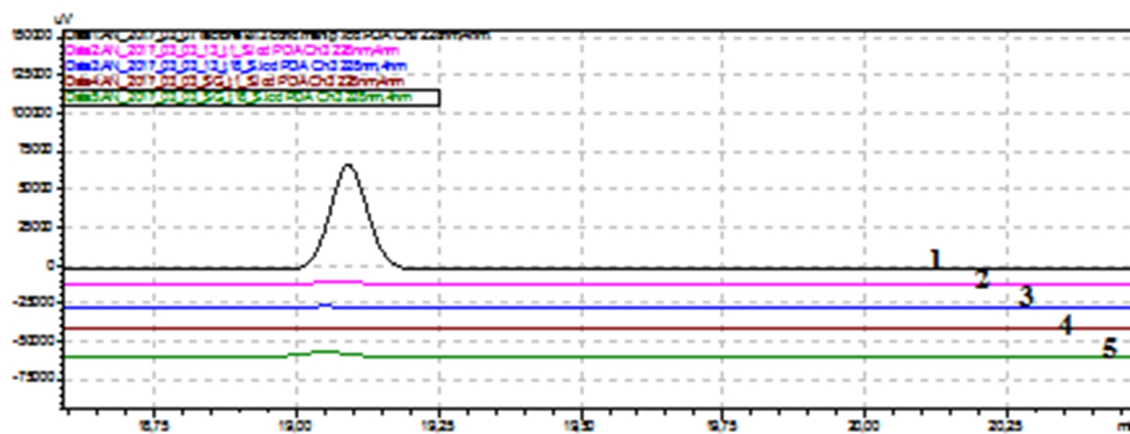
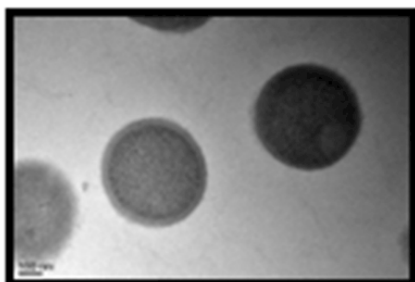


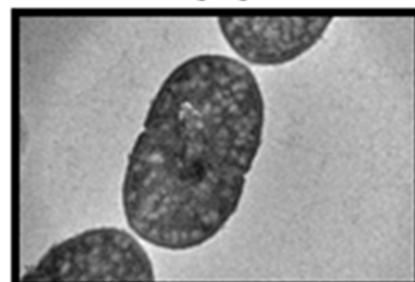
Fig. 3.

S. gordoni

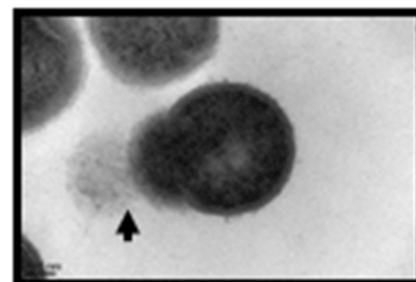
Untreated



Doxycycline



B-13



B-12

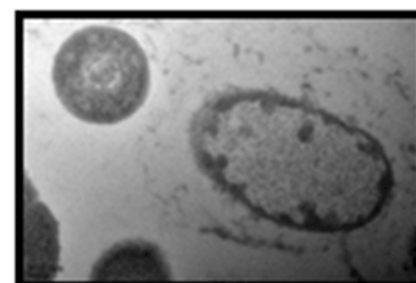
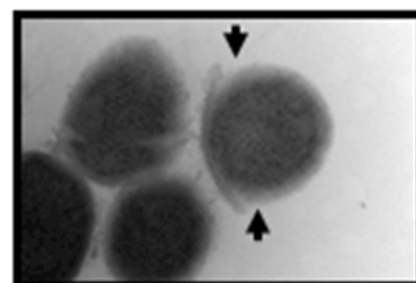
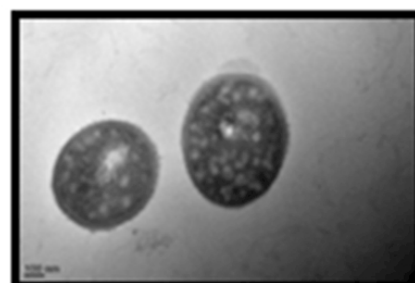
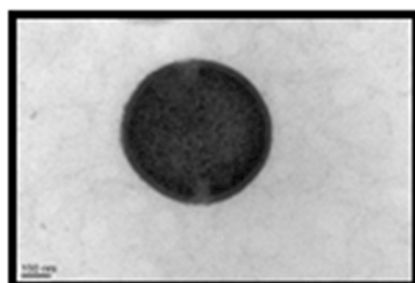
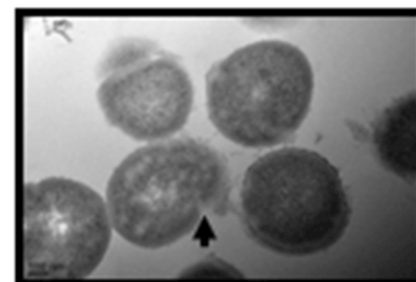


Fig. 4.

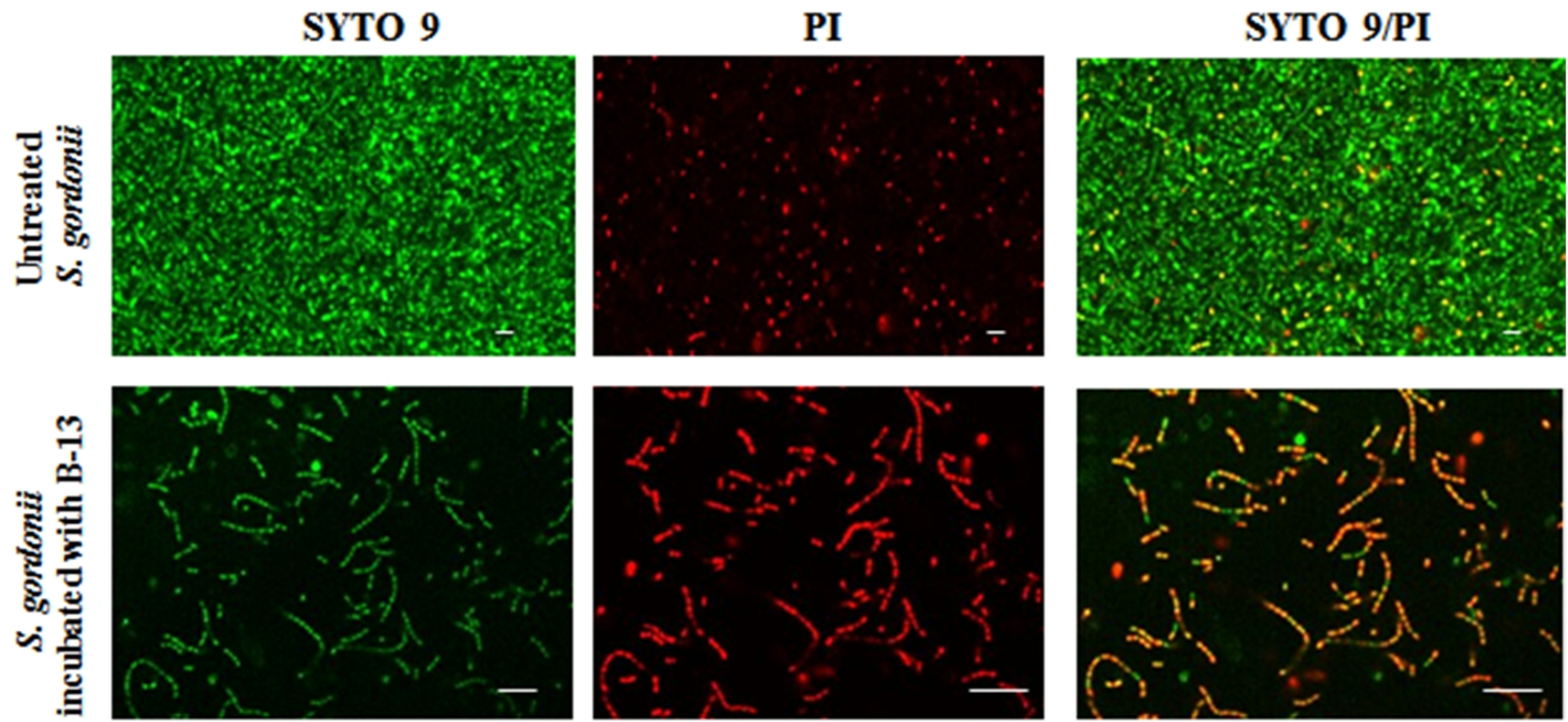


Fig. 5.

Table 1. MIC and MBC of butyrolactones against *P. gingivalis* by broth microdilution

Compound	MIC ($\mu\text{g/mL}$)	MBC ($\mu\text{g/mL}$)
B-1	9.38	37.5
B-2	37.5	150
B-3	4.69	37.5
B-4	4.69	75
B-5	37.5	75
B-6	2.34	75
B-7	75	>i
B-8	9.38	150
B-9	37.5	150
B-10	0.073	9.38
B-11	0.586	4.69
B-12	0.037	1.17
B-13	0.293	0.586
Doxycycline	0.13	>i

>i: greater than the initial concentration

Table 2. Percentage of damaged bacterial cells upon treatment with butyrolactones or doxycycline (enumerated in the transmission electron micrographs).

	<i>S. gordonii</i>	<i>P. gingivalis</i>
B-12	58.5±1.3	92.5±2.8
B-13	55.7±1.6	86.1±3.1
Doxycycline	32.6±2.6	66.4±1.2